Kinematic Calibration by Means of a Triaxial Accelerometer

Gaetano Canepa John M. Hollerbach Alexander J. M. A. Boelen

Biorobotics Laboratory, McGill University,
3775 University St., Montreal, PQ, Canada, H3A 2B4

Abstract

A new method for kinematic calibration of a robot is presented, based on triaxial measurement of acceleration by a sensor fixed to the robot end-point. The kinematic parameters are evaluated by means of a series of simple tests (two for each joint). In these tests each joint, except the one under consideration, is kept fixed. Acceleration and encoder output are then acquired. Simulations and experimental results applied on Sarcos Dextrous Arm are presented to verify this method.

1 Introduction

The availability on the market of new, very accurate, accelerometers gives the possibility to use them as position tracking sensors. This approach to position sensing has various advantages:

- accurate inertial sensors can be less expensive than position sensors;
- accelerometers do not suffer obstruction of track point like optical position sensors;
- accelerometers can also give an accurate measurement of speed and, of course, of acceleration.

This paper presents a method to calibrate a 7 degree of freedom (DOF) robotic arm using a triaxial accelerometer. An open-loop calibration procedure, Circle Point Analysis (CPA) [1, 2], is followed to determinate the kinematic parameters of the Sarcos Dextrous Arm (Sarcos Research Corp., Salt Lake City, Utah). Advantages in the use of inertial sensors, compared to external position sensing systems, include lower cost and lack of viewing or access constraints. Compared to closed-loop calibration, contact forces do not need to be regulated.

CPA involves determination of the DH parameters by movement of one joint at a time. By detecting the movement of an endpoint target, the screw axis for each joint i is estimated (see Figure 1):

$$\begin{bmatrix} \mathbf{z}_{i-1} \\ \mathbf{b}_i \times \mathbf{z}_{i-1} \end{bmatrix}$$

where

$\mathbf{z}_{i-1}$ is the rotation axis for joint i, and

$\mathbf{b}_i$ is any vector from axis $\mathbf{z}_{i-1}$ to the accelerometer.

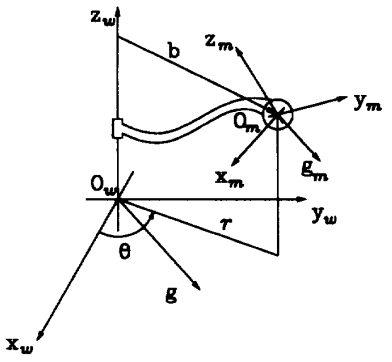

Figure 1: Reference frames $\mathbf{O}_w$ and $\mathbf{O}_m$.

Using these vectors it is possible to determinate all of the DH parameters with the exception of s_0 and θ_0. These last parameters are arbitrary because base coordinate placement is.

This paper only considers manipulators with rotary joints (as the joints on the Sarcos Dextrous Arm), although it is possible to find an equivalent method to calibrate prismatic joints.

2 Kinematic model

It is possible to separate the calibration into static and dynamic phases. The static phase calibrates $\mathbf{z}_i$ and the dynamic one calibrates $\mathbf{b}_i$.

2.1 Axis orientation calibration

The model of the accelerometer data is quite simple when we deal with static measurement of gravity. We assume our model has a generic joint axis $\mathbf{z}$ at a distance r from the accelerometer. Define the following coordinate systems.

$\mathbf{O}_a$ is the accelerometer reference system when the joint is against one of the mechanical stops, with axes $\mathbf{x}_a$, $\mathbf{y}_a$, $\mathbf{z}_a$.

$\mathbf{O}_m$ is the accelerometer reference system after the joint has been rotated by an angle θ from the mechanical stop.

$\mathbf{O}_w$ is a reference system on the joint axis, with axes $\mathbf{x}_w$, $\mathbf{y}_w$, $\mathbf{z}_w$.

The rotation matrix $\mathbf{R}_a$ describes the transformation from $\mathbf{O}_w$ to $\mathbf{O}_a$

$$\mathbf{R}_a = [{}^a\mathbf{x}_w \ {}^a\mathbf{y}_w \ {}^a\mathbf{z}_w] \tag{1}$$

where the superscript a indicates that the vector is represented with respect to frame $\mathbf{O}_a$. During tests the orientation of the accelerometer reference frame changes because of rotation from $\mathbf{O}_a$ to $\mathbf{O}_m$. The corresponding rotation matrix will be (see Figure 1):

$$\mathbf{R}_m = \begin{bmatrix} \cos\theta & \sin\theta & 0 \\ -\sin\theta & \cos\theta & 0 \\ 0 & 0 & 1 \end{bmatrix}$$

Assume that gravity is written as the vector ${}^w\mathbf{g}$, ${}^a\mathbf{g}$, and ${}^m\mathbf{g}$ in the reference frame $\mathbf{O}_w$, $\mathbf{O}_a$ and $\mathbf{O}_m$ respectively. With this notation ${}^m\mathbf{g}$ is given by:

$${}^m\mathbf{g} = \mathbf{R}_m {}^a\mathbf{g} = \mathbf{R}_m\mathbf{R}_a {}^w\mathbf{g} \tag{2}$$

Multiplying the left term of equation (2) by ${}^a\mathbf{z}_w^T$ we get

$${}^a\mathbf{z}_w^T \cdot {}^m\mathbf{g} = ({}^w\mathbf{g})_z \tag{3}$$

From equation (3), it is clear that the component of ${}^m\mathbf{g}$ along the ${}^a\mathbf{z}_w$ axis is constant. We can use this result to find the orientation of ${}^a\mathbf{z}_w$ by means of a series of simple static measurements of $\mathbf{g}$ and a minimization algorithm (see section 4).

Given ${}^a\mathbf{z}_w$, if the component of ${}^a\mathbf{x}_a$ orthogonal to ${}^a\mathbf{z}_w$ is non-zero, then we can arbitrarily define ${}^a\mathbf{x}_w$ as the direction of ${}^a\mathbf{x}_a$ orthogonal to ${}^a\mathbf{z}_w$. Otherwise we could take the same direction with regard to ${}^a\mathbf{y}_a$. Finally, we define ${}^a\mathbf{y}_w = {}^a\mathbf{z}_w \times {}^a\mathbf{x}_w$.

2.2 Center of rotation calibration

The determination of the joint axes can be performed by a simple series of static measurements. On the other hand, to measure the center of rotation we need to perform a dynamic measurement of the acceleration. The information given by the rotation of the joint is sufficient to establish the position of the rotation center. If we rotate the joint we can predict the output $\mathbf{a}_m$ furnised by the sensor with the simple model

$$\mathbf{a}_m = \mathbf{g}_m + \mathbf{a}_r + \mathbf{a}_\theta, \tag{4}$$

where $\mathbf{a}_r$ is the radial component of the acceleration and $\mathbf{a}_\theta$ is the angular component. As from our static measurements, we already know the value of $\mathbf{g}_m$, so we can obtain

$$\hat{\mathbf{a}}_m = \mathbf{a}_r + \mathbf{a}_\theta. \tag{5}$$

From equation (5) it turns out that there is no acceleration along the rotation axis. Consequently, to minimize the noise that affects the measurements, we will project the acceleration on a plane $\mathbf{x}_w - \mathbf{y}_w$ perpendicular to the rotation axis. To simplify the following calculations, we will change the reference frame for the acceleration using the rotation matrix $\mathbf{R}_a^T$. Acceleration is measured in a reference frame that changes orientation during measurement. To have acceleration

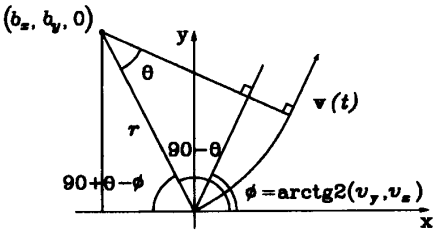

Figure 2: Angular relation useful for center of rotation calibration

in the fixed reference frame $\mathbf{O}_w$, we need to use the information given by the encoder applying the rotation matrix $\mathbf{R}_a^T$ to $\mathbf{R}_m^T\hat{\mathbf{a}}_m$:

$${}^w\hat{\mathbf{a}}_m = \mathbf{R}_a^T\mathbf{R}_m^T {}^m\hat{\mathbf{a}}_m. \tag{6}$$

Acceleration in equation (6) has both radial and tangential components, and these components depend on the value of r, ω, and $\dot{\omega}$. If equation (6) is integrated an equation far more useful for calibration purposes can be obtained:

$$\int_0^t {}^w\hat{\mathbf{a}}_m(\tau)d\tau = {}^w\mathbf{v}(t) - {}^w\mathbf{v}(0) = r\,\omega\,\mathbf{i}_\theta - r\,\omega(0)\,\mathbf{i}_{\theta 0}. \tag{7}$$

where $\mathbf{i}_\theta$ is in the direction of the tangential velocity. As we start our measurements at zero angular velocity w, $\mathbf{v}_w(0)$ and $r\,\omega(0)$ are equal to zero. From equation (7) there are two possible methods to extract the value of $\mathbf{b}$. The first method is based on a successive integration of equation (7), from which

$$\int_0^t\int_0^t {}^w\hat{\mathbf{a}}_m(\tau)\,d\tau\,d\tau = \int_0^t {}^w\mathbf{v}(\tau)\,d\tau = {}^w\mathbf{x}(t) - {}^w\mathbf{x}(0). \tag{8}$$

From these position data it is relatively easy to find the point around which the accelerometer turns using a least squares routine. This method is relatively straightforward but presents a problem when the bias of the accelerometer is high. As we need to integrate two times a signal, the bias error of this signal become very important as time goes on.

The second method is based on the estimation of the modulus of angular velocity from the encoder data differentiation:

$$\frac{d\theta(t)}{dt} = w(t).$$

Using this estimated angular velocity and the result of equation (7), we can easily determine r as:

$$r = \frac{|\int_0^t {}^w\hat{\mathbf{a}}_m(\tau)d\tau|}{w(t)}.$$

Using this estimated r and the angular relation illustrated in Figure 2, it is possible to estimate the

position of $\mathbf{b}$:

$$\mathbf{b} = \begin{bmatrix} r\cos(90+\theta-\phi) \\ r\sin(90+\theta-\phi) \end{bmatrix}.$$

Both r and $\mathbf{b}$ can be better estimated if we use a least squares algorithm to fit all our significant data (where $\mathbf{v}$ is different from zero). This second method is less affected by bias (we integrate acceleration only one time). However, the determination of $w(t)$ is difficult because of the encoder data differentiation. On the other side, because of our knowledge of the movement law, we can use some optimization method to differentiate the encoder. In the following section, we analyze both methods taking into consideration the error on $\mathbf{b}$. Anyway, both methods can be used depending on the quality of the angular displacement sensors on the joint and on the quality of the accelerometers.

An important problem related with the actual realization of a triaxial accelerometer still needs to be analyed. Each accelerometer measures acceleration along a given axis. Combining three accelerometers in a mounting frame with their axes perpendicular and coincident, it is possible to have a triaxial accelerometer. The problem is that they do not measure the acceleration at the intersection of the perpendicular axes but at a point (called *center of percussion*) somewhere down each measurement axis (see Figure 4). As a consequence, during our tests, the accelerometers were measuring a component of acceleration due to the rotation of the mounting frame. If the accelerometers are well built and are assembled on a mounting frame designed and machined with high accuracy, we can suppose (as in our case) that all accelerometers measure the acceleration of a point at a distance d from the point of intersection of their axes. Errors due to the rotation of the reference frame can then be easily calculated. It is a pure centripetal acceleration in which the radius of rotation is the distance of the center of percussion from axis $\mathbf{z}_w$. As an example, for the accelerometer posed along the $\mathbf{x}_a$ axis:

$$d_x = d\,|\mathbf{x}_a \times \mathbf{z}_w|. \tag{9}$$

The component due to the tangential acceleration imposed by the rotation disappears because sensors are sensitive only to acceleration along their respective axes. From (9) the correction term due to d is given by:

$$(a_{x_m})_{corr} = d_x\,|w^2|. \tag{10}$$

After an initial estimation of w, and given a knowledge of d, it is therefore possible to correct the accelerometer reading and find a more accurate estimation of w and $\mathbf{b}$. Only a few iterations are necessary to obtain convergence.

3 Physical system description

The experimental system is composed of three fundamental parts (see Figure 3):

- the sensor,
- the robot under calibration, and
- the control and acquisition unit.

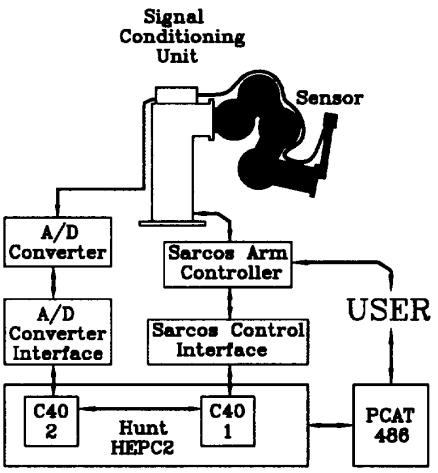

Figure 3: A schematic of the experimental system

3.1 The sensor

The basic component of the triaxial accelerometer is the QA700 accelerometer from Sundstrand Data Control, Inc. This model has an internal temperature sensor and is provided with a set of coefficients of a third order model that provides correction for temperature sensitivity on both bias and scale factor. This assures a control on bias variation with or without high temperature changes. The QA700 is the cheapest in this line of models. Moreover, it has good characteristics with regard to noise and axis misalignment (see Table 1).

These accurate sensors are mounted together on a frame (see Figure 4) machined using a CNC machine with a minimum step of 1 μm. This assures that the axes of the accelerometers are coincident at a point and are perpendicular. The frame is made of aluminum and is designed to be as light as possible, maintaining at the same time high rigidity. The sensor has a handle to connect it to the robot. This handle is 0.5 m long to enable accurate calibration also in case of short links. The sensor and its handle weigh 6.55N and 7.38N respectively (see Figure 5). The output of the sensor is sent to a conditioning unit that filters and amplifies the acceleration and temperature signal and then sends its output to the A/D converter unit, connected with the central processing unit (see Figure 3). The conditioning unit is designed to have a negligible impact with regard to noise and bias sensor characteristic deterioration. The filter used on acceleration signals has a bandwidth of 250 Hz and the one used for the temperature signal has a bandwidth of 1 Hz. The sampling frequency on acceleration signals is 500 Hz.

The actual accelerometers are different from the mathematical model. They have a series of errors that cumulatively contribute to the final measurement error. First of all there is noise on the measurement. This is due to two principal causes:

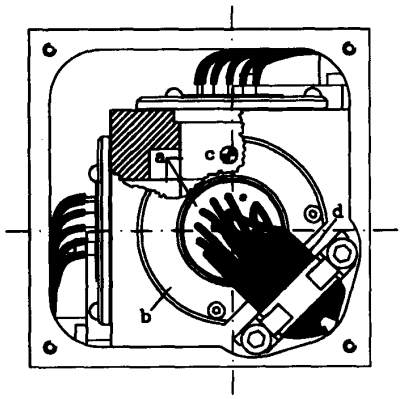

Figure 4: A drawing of the triaxial accelerometer. In the Figure: **a**) accelerometers, **b**) flange fixing accelerometers to the frame, **c**) center of percussion position inside the sensor, **d**) connecting wires.

Figure 5: Photograph of sensor, cables, and signal conditioning unit

- electrical noise, that we can model using white Gaussian noise of given standard deviation and that depends on the circuit bandwidth.

- Environmental noise, that is not white and whose amplitude is usually higher than the electrical noise. This noise depends on vibration amplitude and could have some frequency components higher than others. Environmental noise is included in the simulation using sinusoidals wave of zero mean and different amplitude for each $\mathbf{O}_w$ axes. The amplitude was higher along the tangential direction because of the high rigidity of the arm along the other axes.

Other sources of error are the output nonlinearities (related to the acceleration along the accelerometer axis and along the orthogonal one) and axis misalignment (see Table 1). There are also errors due to the scale factor and bias variations caused by temperature variations (greatly compensated with temperature modeling) and errors due to the sensor working life.

The distance d from the accelerometer center which also causes errors as stated previously is 18.2 $\pm$0.25 mm. All these errors were considered in the preliminary feasibility simulation shown in the following section.

3.2 The robot under calibration

We tested our calibration method on the Sarcos Dextrous Arm which is a 7 degree of freedom anthropomorphic robotic arm [3, 4]. This arm is hydraulically actuated and is furnished with its first 5 links equipped with encoders with interpolation boxes capable of a resolution of 400,000 counts per revolution. The arm is controlled by means of a controller that can be used both in local and remote modes. In the remote mode the arm is controlled by the CPU using both built–in analog or external digital control algorithms. A single link can be moved and have encoder data read at a frequency of 1 kHz. Position of the arm is specified by the analog built-in PD controller.

3.3 The control and acquisition unit

The control and acquisition unit is made up of four components:

- a PC AT–486 which is used as the user interface;

- a Hunt HEPC2 PC Board using two C40 DSP Texas Instruments processors, that control the arm and acquire data;

- a PC board to interface the first C40 processor to the arm and

- a PC board to interface the second C40 processor to the A/D converter which collects signals from the sensor.

The A/D converter is a DT5741-PGH programmable module. We use it in the non–overlapped mode enabling the board to acquire data from a random channel at a frequency of 40 kHz. The two C40 processors work in parallel at a clock frequency of 40 MHz and are connected by means of two 8 bit comports capable of a transfer rate of 20 Mbit per second. All the acquisition and arm control programs are written in Parallel C 3L Ldt (Edimburgh, Scotland).

4 Algorithms and simulations

Simulations were performed before sensor design and construction to test the feasibility of the calibration method. Care was taken to include every possible calibration error into the simulation model. Starting from the QA700 characteristics (Table 4), the model also includes the error due to the distance d and the angular displacement error caused by the discrete encoder readings.

Output Range:	$\pm$ 300 m/s^2
Bias:	80 mm/s^2 max
Bias Thermal Coefficient:	700 μm/s^2 ^{o}C max
Residual Bias error:	200 mm/s^2 max
Current Scale Factor:	.13 mA s^2/m nom
Scale Factor Thermal Coef.:	200 ppm/^{o}C max
Residual Scale Factor Error:	200 ppm/^{o}C max
Second Order Nonlinearity:	4.8 μs^2/m max
Axis Misalignment:	< 2 m rad
Resolution/Threshold:	< 10 μm/s^2
Frequency Response:	
0–10 Hz	● 0.1 % max
10–200 Hz	$\pm$ 5 % max
200–300 Hx	$\pm$ 10 % max
Noise:	
0–10 Hz	< 80 μm/s^2 rms
10–500 Hz	< 800 μm/s^2 rms

Table 1: Sensor characteristics (From Sundstrand data sheet)

As a first step, the maximum limiting error is determined. To calculate this error the measured acceleration is written as:

$$a_m = a + n = a + w + p$$

where n is the cumulative noise and is divided into two parts: w, white gaussian zero mean noise, and p, a non-zero mean error which includes the effects of nonlinearity, bias, and scale factor.

Static measurements indicate an environmental noise standard deviation of approximately 0.5 mm/s^2. The worst value for $\mathbf{p}$ is found from sensor characteristics and can be maximized with the value $p = 5$mm/s^2 for static measurements. With this value for p and w it is possible to bound the $\mathbf{g}$ orientation (using 150 measurements) with

$$\Delta\phi \leq \frac{\varepsilon_m}{g} \leq \frac{\varepsilon_w + \varepsilon_p}{g} \approx 5.6 \times 10^{-4} rad$$

where ε_w is three times the standard deviation of w and ε_p is the maximum error p. The maximum error on the axis determination will be less than $\Delta\phi$, considering the benefical effect of least squares on the random noise component ε_w.

Applying $\Delta\phi$ to an arm with a workspace radius of 1 m gives a maximum endpoint position error of 5.6×10^{-4} m. To determine a maximum error with regard to the vector $\mathbf{b}$ is more difficult because it depends on bias variation between static and dynamic tests, and on structural vibration. Vibration creates an unknown increase in w. Actual measurement is the only method for determining the real noise level. It is anyway reasonable to use the same value as in the static test for bias error, a standard deviation of 10 mm/s^2 on $\hat{\mathbf{a}}_m$, and sinusoidal component with different amplitude, frequencies and phases for simulations. The real situation is in fact that the bias is lower than in the static measurements because of the subtraction between dynamically measured acceleration and previously statically measured gravity plus bias.

In fact the simulation results show an error level lower than the calculated maximum bound, as expected because of the really rough estimation.

The simulation algorithm is written in C. Using equations (1–4,10) and the angular displacement equation (11) in the next section, acceleration data $(\mathbf{g}_m)_i$, $(\mathbf{a}_m)_i$ and the encoder data $(\theta)_i$ are generated. Using the supplied sensor data sheet, errors (w and p data) are added by using the same bias as $\mathbf{g}_m$ and $\mathbf{a}_m$ measurements (assuming measurements are made at the same temperature). To take into account vibration, sinusoidal components with amplitude of 100 mm/s^2 along axis tangential to the trajectory, and 10 mm/s^2 along the orthogonal axes are also added. The axis misalignment error is not considered because the real orientation errors of the accelerometer axes is less then 0.05 mrad. For different situations, it is possible to design a different mounting frame which permits compensation for the accelerometer axis misalignment.

The ${}^a\mathbf{g}$ data are obtained. The ${}^a\mathbf{z}_w$ orientation takes the form ${}^a\mathbf{z}_w = [l\ m\ n]$, from which it can be written:

$${}^a\mathbf{z}_w \cdot ({}^a\mathbf{g})_i - ({}^w\mathbf{g})_z = w_i + p_i,$$

where w_i and p_i are the components of the error for the ith measurement. Minimizing the function

$$\sum_{i=1}^{N} [l({}^a g_x)_i + m({}^a g_y)_i + \sqrt{1 - l^2 + m^2}\,({}^a g_z)_i - {}^w g_z]^2$$

under the condition $1 - l^2 + m^2 > 0$ we obtain the direction ${}^a\mathbf{z}_w$. Errors on ${}^a\mathbf{z}_w$ calibration on ten trials are a maximum orientation error of 0.3 mrad and a standard deviation of 0.1 mrad. These errors are well inside the maximum error bound because of the rough estimation of the bound.

The vector ${}^m\hat{\mathbf{a}}_m$ is projected onto a plane perpendicular to $\mathbf{z}_w$ and rotated to the ${}^a\mathbf{O}_w$ reference frame using equation (6).

Using the TRAP integration method, we then integrate the acceleration data twice to obtain position data. From position data a point on the rotation axis in the reference frame $\mathbf{O}$ is found using a circle interpolation rule.

With this first estimation of r, data are reanalyzed taking into account the error d. The angular velocity estimated from equation (7) is used to calculate the error in acceleration data. After two iterations there was no further improvement in accuracy. The results from 10 tests show a maximum error of 3 mm and standard deviation of 2 mm on the determination of the center of rotation (COR).

As a second method, the encoder data are used to estimate w and r (performing iteration again). The angular velocity data is filtered and r is estimated using the equation

$$r = \text{mean}\left[\frac{|\int_0^{t_i} ({}^w\hat{\mathbf{a}}_m)_i\, d\tau|}{w_i}\right].$$

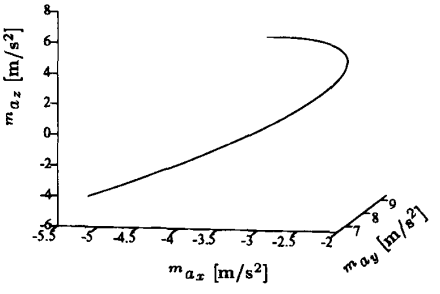

Figure 6: Output of the accelerometer during a static measurement.

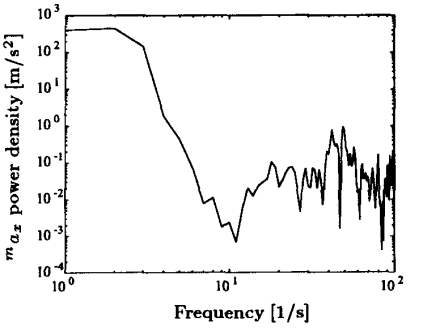

Figure 7: Power spectrum of the accelerometer during a dynamic measurement.

Using r and the velocity data (produced by the first integration of acceleration data) the center of rotation is obtained by:

$$x_c = r\,\mathrm{mean}[cos(90 + \theta_i - \phi_i)]$$

$$x_c = r\,\mathrm{mean}[sin(90 + \theta_i - \phi_i)].$$

Results are slightly better than the ones of the first method (maximum error of 3 mm and standard deviation of 2 mm on the determination of COR).

5 Experimental results

The experimental phase is divided into two parts: the static determination of **g** for the calibration of the rotation axis, and a dynamical test to determine a vector **b**. The test has been performed only on the first and second joints of the Sarcos Dextrous Arm and the simulation algorithms were used to analyze the collected data. To identify the direction of **g** at various encoder angles, the joint under consideration is moved one degree at a time. We wait at every position 3 seconds for the oscillation of the arm to stop and then we collect during 1 second the accelerometer outputs. Using this procedure ambiental noise is reduced to 0.1 mm/s^2. Collecting both ^{a}**g** and the encoder output we have all the information required to exclude gravity from successive acceleration measurements.

In our experiment we repeat this phase 10 times to test the repeatability and the error in identification of the axis directions. We found a maximum error of 0.3 mrad and a standard deviation of 0.1 mrad, in according with simulation results. Figure 6 shows the variation of the acceleration measured by the sensor during the rotation of the second joint.

The nominal angle α between the first two joint axes of the Sarcos Dextrous Arm is 90^o. We found that the two axes have a misallignment error of 0.4 $\pm$ 0.3 mrad.

Collecting both ^{a}**g** and the encoder output we have all the information required to exclude gravity from successive acceleration measurements.

Using data about ^{a}**g**, we performed the second phase of the calibration. We moved the arm approximately with a sinusoidal law of the angular displacement:

$$\theta = \theta_0 + \theta_s(1 - \cos(2\pi f_0 t))/2. \qquad (11)$$

In our experiments f_0 had a value of 0.5 Hz, the spanned angle θ_s a value of 150 degrees, and the sampling frequency 500 Hz.

This displacement law is imposed in order to facilitate filtering of angular displacement and acceleration, considering that the fundamental frequency of the signal, f_0, is much higher than the other components. A digital filter (with no phase shift) was then applied to the data. Looking at the power spectrum of $^m a_x$ shown in Figure 7, we decided to filter data with a bandwidth of 10 Hz, to take into account some harmonics of $\theta(t)$. Figure 7 indicates that some oscillations arise caused by the movement of the arm.

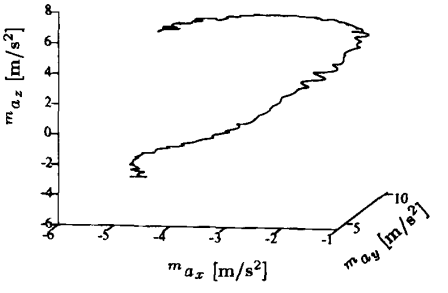

Figure 8: Output of the accelerometer during a dynamic measurement

In Figure 8 is shown the triaxial output of the accelerometer filtered with a Butterworth filter with corner frequency of 20 Hz, and Figure 9 the corresponding reconstructed trajectory of the accelerometer's center. Oscillation are clearly visible in acceleration while accelerometer trajectory is quite smooth. In Figure 10 is shown the filtered output of the differentiation of θ.

Applying the two different algorithms described in

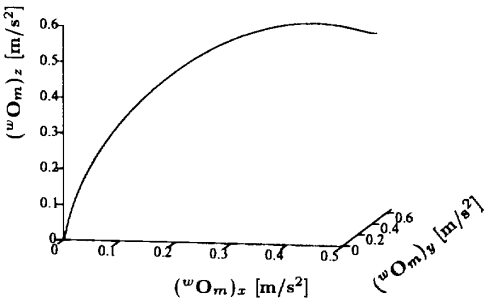

Figure 9: Trajectory of the accelerometer center in $\mathbf{O}_w$ reference system

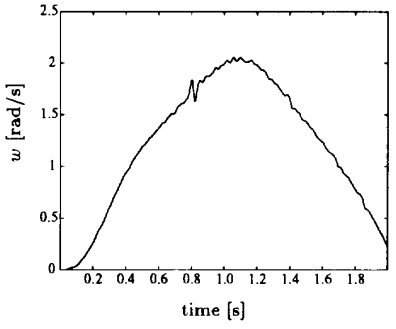

Figure 10: Angular velocity of the joint obtained filtering encoder data with a low-pass filter with corner frequency 20 Hz and then differentiating them

the preceding section to the 10 tests we found an error of 1.5 cm on COR position. This error is quite big, and is due to a series of factors:

- low sampling frequency;
- cable length picking up a considerable amount of noise;
- distance of the accelerometer less than 0.4 m from the rotation center.

Taking into account all these factor into the simulation the resulting error was of the same order.

6 Discussion

The error (rms) on parameter estimation was 1.5 cm on the position of center of rotation, and of 0.3 mrad on the orientation of the axes, with an estimated end-point cumulative error of 15 mm. Simulations points out that this accuracy could be increased using a higher class of accelerometer. For example the QA3000, the most accurate accelerometer of Q-flex series of Sundstrand Aerospace, has better performance with regard to noise, bias, axis misalignment and temperature compensation. The most important improvement to the measurement system will be to place the conditioning circuit and the A/D converter closer to the accelerometer, because noise picked up along the cable will be eliminated. A higher sampling frequency could greatly improve the accuracy of the integration algorithm. We are right now in the process of implementing these improvements.

With regard to the model of the arm, it should be possible to implement a more complicated one including mechanical geometrical imperfections like link compliance and robot base motion [5]. In the future this work will be extended to the estimation, by means of a triaxial accelerometer of both kinematic and inertial parameters.

Acknowledgment

Support for this research was provided by Office of Naval Research Grant N00014-90-J-1849, and by the Natural Sciences and Engineering Research Council (NSERC) Network Centers of Excellence Institute for Robotics and Intelligent Systems (IRIS). Personal support for JMH was provided by the NSERC/Canadian Institute for Advanced Research (CIAR) Industrial Chair in Robotics. G. Canepa is supported by a Government of Canada Award, administered by the International Council of Canada Studies.

References

[1] D. J. Bennett, J. M. Hollerbach, and P. D. Henri. Kinematic calibration by direct estimation of the jacobian matrix. In *IEEE Intl. Conf. Robotics and Automation*, pages 351–357, Nice, May 10–15 1992.

[2] J. M. Hollerbach, L. Giugovaz, M. Buehler, and Y. Xu. Screw axis measurement for kinematic calibration of the sarcos dextrous arm. In *Proc. IEEE/RSJ Intl. Conf. on Intelligent Robots and Systems*, pages 1617–1621, Yokohama, Japan, July 26–30 1993.

[3] S. C. Jacobsen, F. M. Smith, D. K. Backman, and E. K. Iversen. High performance, high dexterity, force reflective teleoperator ii. In *ANS Topical Meeting on Robotics and Remote Systems*, Albuquerque, NM, Feb. 24–27 1991.

[4] S. C. Jacobsen, F. M. Smith, E. K. Iversen, and D. K.Backman. High performance, high dexterity, force reflective teleoperator. In *Proc. 38th Conf. Remote Systems Technology*, Washington, DC, Nov. 1990.

[5] D. E. Whitney, C. A. Lozinski, and J. M. Rourke. Industrial robot forward calibration method and results. *Journal of Dynamic Systems, Measurement, and Control*, pages 1–8, Mar 1986.